Radiation and chemical reaction effects on MHD Casson fluid flow past a semi-infinite vertical moving porous plate

A Sandhya[a,b]*, G Venkata Ramana Reddy[c] & G V S R Deekshitulu[a]

[a]Department of Mathematics, Jawaharlal Nehru Technological University, Kakinada 533 003, India
[b]Department of Mathematics, VR Siddhartha Engineering College, Kanur, Vijayawada 520 007, India
[c]Department of Mathematics, Koneru Lakshmaiah Educational Foundation, Vaddeswaram 522 502, India

A speculative investigation has been presented to explore the significant features of MHD convective Casson fluid flow past a semi-infinite moving vertical porous plate with heat source/sink are included in the flow configuration. The governing partial differential equations are remodeled into ordinary differential equations using appropriate non-dimensional variables. The ensuing differential equations are solved analytically using two term perturbation technique method. The result of flow heat and mass transfer analysis on the velocity, temperature and concentration profiles and also physical parameters like Skin friction, Nusselt number, and Sherwood numbers are shown graphically, also shown in tabular form. The results shows that Casson parameter enhances the velocity, temperature and concentration fields are decreases for increasing the values radiation and chemical reaction. Under some restriction the resultant outcome were compared with previous published results and is found in admirable agreement.

1 Introduction

The analysis of non-Newtonian Casson fluid can be described as a shear thinning liquid at zero rate of shear having an infinite viscosity, at an infinite rate of shear, a yield stress below having zero viscosity and no flows occurs. If a yield stress greater than the shear stress is applied to the fluid, it behaves like a solid, where as if a yield stress less than shear stress is applied and it starts to move. This is widely used for modeling blood flow in narrow arteries. Many researchers have used the Casson fluid model for mathematical modeling of blood flow in narrow arteries at low shear rates. Few examples of Casson fluids are tomato sauce, jelly, concentrated fruit juice, honey, blood etc.

Shehzad *et al.*[1] described the mass transfer effects on MHD Casson fluid flow with chemical reaction. Vajravelu *et al.*[2] analyzed in flow of the casson fluid dispersal of chemically reactive species over permeable an unsteady stretching surface. Abid *et al*.[3] discussed unsteady heat transfer and boundary layer flow of a Casson fluid past an oscillating Newtonian heating with vertical plate. Sekhar *et al.*[4] analyzed convective heat and mass transfer of unsteady MHD Casson fluid past a permeable semi-infinite vertical

moving plate with heat source/sink. Animasaun[5] developed effects of thermal conductivity, variable viscosity and thermophoresis on Non-Darcian MHD free convective heat and mass transfer of dissipative Casson fluid flow with nth order of chemical reaction and suction. Suresh *et al.*[6] studied effect of radiative and dissipative free convective heat transfer flow of a Casson fluid due to variable internal heat generation and thermal conductivity past a stretching sheet. Falodun *et al.*[7] computed numerically heat transfer on unsteady incompressible magnetohydrodynamic (MHD) boundary layer fluid flow of a vertical moving plate. Falodun[8] studied the effect of thermophoresis on MHD heat and mass transfer flow past of Casson fluid a semi-infinite vertical plate. Makinde *et al.*[9] discussed the effect of chemical reaction on MHD Casson fluid flow with porous stretching sheet. Rama Krishna Reddy *et al.*[10] presented Free convective MHD flow past a porous plate. Nagasantoshi[11] studied heat and mass transfer of non-Newtonian flow of Nano fluid over a stretching sheet with non-uniform variable viscosity and heat source. Gvrreddy[12] discussed Soret and Dufour effects on flow of MHD micropolar fluid through a non-Darcy porous medium over a linearly stretching sheet. Suneetha *et al.*[13] represented effects of heat source and radiation effects on MHD flow

*Corresponding author (E-mail: akuri.sandhya@gmail.com)

through porous stratum over a permeable stretching sheet with chemical reaction. Vijaya *et al.*[14] developed effects of radiation and Soret on an unsteady Casson fluid flow through vertical porous channel with contraction and expansion. Ramana Reddy *et al.*[15] represented numerical solutions of unsteady heat transfer MHD flow over a stretching surface with injection or suction.

In view of these an investigation, the major concerns of present pattern are to consider the magnetohydrodynamic convective Casson fluid flow past a semi-infinite vertical moving porous plate with heat source/sink are included in the flow.

In most of the previous works semi-infinite plate kept at rest. In the present work, it is assumed that the plate is embedded in a uniform porous medium and moves with a constant velocity in the flow direction in the presence of a transverse magnetic field under the influence of radiation and chemical reaction effects. The mathematical modelling of flow arrangement yields simultaneous non-linear partial differential equations. The appropriate two term perturbation technique method employed to governing equations to deduce two non-dimensional ordinary differential equations. The numerical values of the physical parameters like Skin friction, Nusselt number, and Sherwood number are shown graphically, also presented in tabular form.

2 Mathematical Analysis

We consider an unsteady two-dimensional free convective MHD flow of a viscous, an electrically conducting, heat absorbing and incompressible fluid past a semi-infinite permeable vertical plate insert in a uniform porous medium which having boundary condition at the collaborate of fluid layers and porous medium. A uniform transverse magnetic field of strength B_0 is applied perpendicular to the flow direction as shown in the Fig. 1. The effects of radiation, heat source/sink and first-order destructive chemical reactions are considered. The transversely applied magnetic Reynolds number and magnetic field are considered to be very small so that induced magnetic field and Hall Effect are negligible. It is considered that there is no applied voltage which results the deficiency of electric field. The length of the plate is large enough and the motion is two-dimensional so all the physical variables are independent of x'.

The wall is maintained at constant concentration C_w and temperature T_w, greater than the surrounding
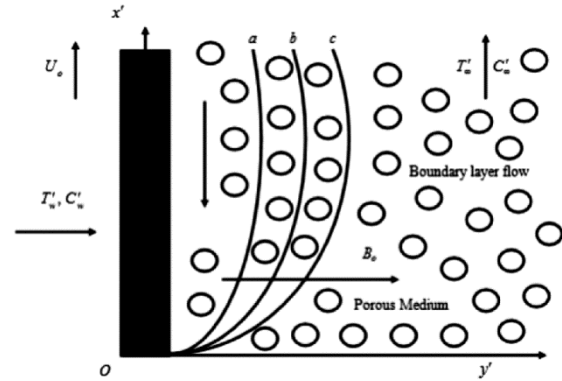

Fig.1 — Physical configuration of the problem.

concentration C'_∞ and temperature T'_∞ , respectively. Also, it is considered that there exists a first-order homogeneous Casson fluid and the heat source. It is considered to be homogeneous porous and exist everywhere in local thermodynamic equilibrium. Remaining properties of the porous medium and the fluid are taken to be constant.

For an isotropic flow of a Casson fluid, the rheological equation of state is given:

$$\tau_{ij} = \begin{cases} 2\left(\dfrac{\mu_B + P_{y'}}{\sqrt{2\pi}}\right)e_{ij}, \ \pi > \pi_c, \\ 2\left(\dfrac{\mu_B + P_{y'}}{\sqrt{2\pi_c}}\right)e_{ij}, \ \pi < \pi_c, \end{cases}$$

where $\pi = e_{ij}e_{ij}$ and e_{ij} is the $(i,j)^{th}$ distortion rate component, π is the resulted from rate of distortion with itself, the product π_c is a critical value reliant upon the non-Newtonian model, μ_B is the non-Newtonian viscosity relevant to a plastic dynamic fluid and P_y is the yield fluid pressure. Under these assumptions, the governing equations can be expressed as:

$$\frac{\partial v'}{\partial y'} = 0 \qquad \qquad \dots (1)$$

$$\frac{\partial u'}{\partial t'} + v'\frac{\partial u'}{\partial y'} = -\frac{1}{\rho}\frac{\partial p'}{\partial x'} + \nu\left(1 + \frac{1}{\beta}\right)\frac{\partial^2 u'}{\partial y'^2} + g\beta_T\left(T' - T'_\infty\right)$$
$$+ g\beta_C\left(C' - C'_\infty\right) - \frac{\sigma B_0^2}{\rho}u' - \frac{\nu}{k'}u'$$
$$\qquad \qquad \dots (2)$$

$$\frac{\partial T'}{\partial t'} + v'\frac{\partial T'}{\partial y'} = \alpha\frac{\partial^2 T'}{\partial y'^2} - \frac{Q_0}{\rho c_p}\left(T' - T'_\infty\right) - \frac{1}{\rho c_p}\frac{\partial q'_r}{\partial y'} \qquad \dots (3)$$

$$\frac{\partial C'}{\partial t'}+v'\frac{\partial C'}{\partial y'}=D\frac{\partial^2 C'}{\partial y'^2}-Kr\left(C'-C'_\infty\right) \qquad \dots (4)$$

where x' and y' are the dimensional distances along to the plate. u' and v' are the of dimensional velocity components along x' and y' directions. g is the gravitational acceleration, T' is the fluid dimensional temperature near the plate, T'_∞ is the stream dimensional temperature far away from the plate , C' is the dimensional concentration of the fluid, C'_∞ is the stream dimensional concentration far away from the plate. β_T and β_C - expansion coefficients of the thermal and concentration respectively. p' is the pressure, C_p is the specific heat, B_0 is the coefficient of magnetic field, μ is fluid viscosity, ρ is the density, k' is the thermal conductivity, σ is the density of the fluid magnetic permeability, $\nu=\dfrac{\mu}{\rho}$ is the kinematic viscosity, D is the diffusivity of the molecular, Q_0 is the dimensional coefficient of the heat absorption and β is the Casson parameter. The third and fourth terms of RHS of Eq. (2) denote the thermal and concentration buoyancy effects, respectively.

$$u'=U'_p, T'=T'_w+\varepsilon(T'_w-T'_\infty)e^{n't'}, C'=C'_w+$$
$$\varepsilon(C'_w-C'_\infty)e^{n't'} \qquad \text{at} \quad y'=0 \qquad \dots (5)$$

$$u'=U'_\infty=U_0(1+\varepsilon e^{n't'}), T'\to T'_\infty, C'\to C'_\infty$$
$$\text{as} \quad y'\to\infty \qquad \dots (6)$$

where U'_p, T'_w, C'_w, are the wall dimensional velocity, temperature and concentration, respectively. U'_∞, T'_∞, C'_∞, are the free stream dimensional velocity, temperature and concentration, respectively U_0, n' are constants.

The radiative flux vector q'_r can be written by using the Rosseland approximation as:

$$q'_r=-\frac{4\sigma^*}{3k'_1}\frac{\partial T'^4_w}{\partial y'} \qquad \dots (7)$$

where, σ^* and k'_1 are the Stefan-Boltzmann constant and mean absorption coefficient respectively.

We considered that the temperature difference is sufficiently small within the flow such that T'^4 can be represented as a linear function of the temperature. This is obtained by expanding in a Taylor series neglecting higher order terms about the free stream temperature T'_∞, thus

$$T'^4_w\cong 4T'^3_\infty T'_w-3T'^4_\infty \qquad \dots (8)$$

From Eq. (1) the velocity of the suction at the plate surface is a function of time only. Assuming that it takes exponential form as follows:

$$v'=-V_0\left(1+\varepsilon A e^{n't'}\right) \qquad \dots (9)$$

where V_0 is a scale of suction velocity which has non-zero positive constant, A is a real positive constant and ε and εA are small less than unity. Eq. (2) gives the Outside boundary layer

$$-\frac{1}{\rho}\frac{dp'}{dx'}=\frac{dU'_\infty}{dt'}+\frac{\sigma}{\rho}B_0^2U'_\infty+\frac{\nu}{k'}U'_\infty \qquad \dots (10)$$

Let us introducing the non-dimensional quantities

$$u=\frac{u'}{V_0}, v=\frac{v'}{V_0}, y=\frac{V_0 y'}{\nu}, U_\infty=\frac{U'_\infty}{U_0}, t=\frac{t'V_0^2}{\nu}, \theta=\frac{T'-T'_\infty}{T'_w-T'_\infty},$$

$$\phi=\frac{C'-C'_\infty}{C'_w-C'_\infty}, U_p=\frac{u'_p}{U_0}, Sc=\frac{\nu}{D}, K=\frac{k'V_0^2}{\nu^2}, Q=\frac{Q_0\nu}{\rho C_p V_0^2},$$

$$M=\frac{\sigma B_0^2\nu}{\rho V_0^2}, Gr=\frac{\rho\nu g\left(T'_w-T'_\infty\right)\beta_T}{U_0 V_0^2},$$

$$Gc=\frac{\rho\nu g\left(C'_w-C'_\infty\right)\beta_C}{U_0 V_0^2}, \text{Pr}=\frac{\nu}{\alpha}, R=\frac{4\sigma^* T'^3_\infty}{k'_1 k'}$$

$$\dots (11)$$

In the view of the above dimensionless variables, the basic field of Eqs (2) - (4) can be expressed in non-dimensional form as:

$$\frac{\partial u}{\partial t}-\left(1+\varepsilon A e^{nt}\right)\frac{\partial u}{\partial y}=\frac{dU_\infty}{dt}+\frac{\partial^2 u}{\partial y^2}\left(1+\frac{1}{\beta}\right)$$
$$+Gr\theta+Gc\phi-N\left(U_\infty-u\right) \qquad \dots (12)$$

$$\frac{\partial\theta}{\partial t}-\left(1+\varepsilon A e^{nt}\right)\frac{\partial\theta}{\partial y}=\frac{1}{\text{Pr}}\frac{\partial^2\theta}{\partial y^2}-(Q-R)\theta \qquad \dots (13)$$

$$\frac{\partial\phi}{\partial t}-\left(1+\varepsilon A e^{nt}\right)\frac{\partial\phi}{\partial y}=\frac{1}{Sc}\frac{\partial^2\phi}{\partial y^2}-Kr\phi \qquad \dots (14)$$

Where, $N = \left(M + \dfrac{1}{K} \right)$

The corresponding boundary conditions (5) and (6) in non-dimensional form are:

$$u = U_p, \theta = 1 + \varepsilon e^{nt}, \phi = 1 + \varepsilon e^{nt} \text{ at } \text{y=0} \qquad \dots (15)$$

$$u = U_\infty = (1 + \varepsilon e^{nt}), \theta \to 0, \phi \to 0 \text{ as } \text{y} \to \infty \qquad \dots (16)$$

3 Solution of the Problem

Equations (12)-(14) represent a set of partial differential equations that cannot be solved in closed-form. However, it can be reduced to a set of ordinary differential equations in dimensionless form that can be solved analytically. This can be done by representing the velocity, temperature and concentration as:

$$u(y,t) = u_0(y) + \varepsilon e^{nt} u_1(y) + O(\varepsilon^2) + ------ \qquad \dots (17)$$

$$\theta(y,t) = \theta_0(y) + \varepsilon e^{nt} \theta_1(y) + O(\varepsilon^2) + ------ \qquad \dots (18)$$

$$\phi(y,t) = \phi_0(y) + \varepsilon e^{nt} \phi_1(y) + O(\varepsilon^2) + ------ \qquad \dots (19)$$

Substituting Eqs (17)-(19) into Eqs (12)-(14) and equating the harmonic and non-harmonic terms, and neglecting the higher order, $o(\varepsilon^2)$ and simplifying to get the following pairs of equations for u_0, θ_0, ϕ_0 and u_1, θ_1, ϕ_1

$$\left(1 + \frac{1}{\beta} \right) u_0'' + u_0' - N u_0 = -\left[Gr\theta_0 + Gc\phi_0 + N \right] \qquad \dots (20)$$

$$\left(1 + \frac{1}{\beta} \right) u_1'' + u_1' - (N+n)u_1 = -\left[Gr\theta_1 + Gc\phi_1 + Au_0' + N + n \right] \qquad \dots (21)$$

$$\theta_0'' + \Pr \theta_0' - (Q+R)\Pr \theta_0 = 0 \qquad \dots (22)$$

$$\theta_1'' + \Pr \theta_1' - (Q+R+n)\theta_1 = -A\theta_0' \qquad \dots (23)$$

$$\phi_0'' + Sc\phi_0' - ScKr\phi_0 = 0 \qquad \dots (24)$$

$$\phi_1'' + Sc\phi_1' - Sc(Kr+n)\phi_1 = -A\phi_0' \qquad \dots (25)$$

Where the prime denotes ordinary differentiation with respect to y,

The corresponding boundary conditions are:

$$u_0' = u_p', \ u_1' = 1, \ \theta_0' = 1, \ \theta_1' = 1, \ \phi_0' = 1, \ \phi_1' = 1 \text{ as y'=0} \qquad \dots (26)$$

$$u_0' = 1, \ u_1' = 1, \ \theta_0' \to 0, \ \theta_1' \to 0, \ \phi_0' \to 0, \ \phi_1' \to 0 \text{ as y'} \to \infty \qquad \dots (27)$$

without going into the details, the solutions of Eqs. (20)- (25) With the help of boundary conditions (26) and (27), we get:

$$u_0 = A_7 e^{(-m_5 y)} + A_5 e^{(-m_3 y)} + A_6 e^{(-m_1 y)} + 1 \qquad \dots (28)$$

$$u_1 = A_{17} e^{(-m_6 y)} + A_8 e^{(-m_5 y)} + A_{11} e^{(-m_4 y)} + A_{15} e^{(-m_3 y)} + A_{13} e^{(-m_2 y)} + A_{16} e^{(-m_1 y)} + 1 \qquad \dots (29)$$

$$\theta_0 = e^{-m_3 y} \qquad \dots (30)$$

$$\theta_1 = A_4 e^{-m_4 y} + A_3 e^{-m_3 y} \qquad \dots (31)$$

$$\phi_0 = e^{-m_1 y} \qquad \dots (32)$$

$$\phi_1 = A_2 e^{-m_2 y} + A_1 e^{-m_1 y} \qquad \dots (33)$$

In view of the above solutions, the velocity, temperature and concentration distributions in the boundary layer become:

$$u(y,t) = (A_7 e^{(-m_5 y)} + A_5 e^{(-m_3 y)} + A_6 e^{(-m_1 y)} + 1) + \varepsilon e^{nt} (A_{17} e^{(-m_6 y)} + A_8 e^{(-m_5 y)} + A_{11} e^{(-m_4 y)} + A_{15} e^{(-m_3 y)} + A_{13} e^{(-m_2 y)} + A_{16} e^{(-m_1 y)} + 1) \qquad \dots (34)$$

$$\theta(y,t) = (e^{-m_3 y}) + \varepsilon e^{nt} (A_4 e^{-m_4 y} + A_3 e^{-m_3 y}) \qquad \dots (35)$$

$$\phi(y,t) = (e^{-m_1 y}) + \varepsilon e^{nt} (A_2 e^{-m_2 y} + A_1 e^{-m_1 y}) \qquad \dots (36)$$

Here the constants are not given due to the sake of brevity. The Skin-friction coefficient, the Nusselt number and the Sherwood number are significant physical parameters for this type of boundary-layer flow. These parameters can be defined and determined as follows.

4 Skin Friction

In the non-dimensional form the skin friction on the plate $y = 0$, after getting the velocity field is given by:

$$C_f = \frac{\nu\left(1 + \frac{1}{\beta}\right)\frac{\partial u}{\partial y}\Big|_{y=0}}{\rho U_0 V_0} = \frac{\partial u}{\partial y}\Big|_{y=0}$$

$$= -\begin{bmatrix} (m_5 A_7 + m_3 A_5 + m_1 A_6) \\ + \varepsilon e^{nt}(m_6 A_{17} + m_5 A_8 + m_4 A_{11} \\ + m_3 A_{15} + m_2 A_{13} + m_1 A_{16}) \end{bmatrix} \qquad \dots (37)$$

5 Nusselt Number

The heat transfer coefficient can be obtained by the temperature field, which is in non-dimensional form in terms of Nusselt number is given by

$$Nu = x\frac{\frac{\partial \theta}{\partial y'}\Big|_{y=0}}{(T'_w - T'_\infty)} \Rightarrow Nu\,\mathrm{Re}_x^{-1} = \frac{\partial \theta}{\partial y}\Big|_{y=0} \qquad \dots (38)$$

$$= \left[m_3 + \varepsilon e^{nt}(m_4 A_4 + m_3 A_3) \right]$$

where, $\mathrm{Re}_x = \dfrac{V_0 x}{\nu}$ is the Reynolds number

6 Sherwood Number

The rate of mass transfer coefficients can be obtained with the concentration field, in the non-dimensional form in terms of Sherwood number is

given by $Sh_x = x\dfrac{\frac{\partial \phi}{\partial y'}\Big|_{y=0}}{(C'_w - C'_\infty)} \Rightarrow Sh_x\,\mathrm{Re}_x^{-1} = \dfrac{\partial \phi}{\partial y}\Big|_{y=0}$ $\qquad \dots (39)$

$$= -\left[m_1 + \varepsilon e^{nt}(m_2 A_2 + m_1 A_1) \right]$$

7 Results and Discussion

The system of non-linear coupled ordinary differential Eqs (12)-(14) having boundary conditions are solved analytically, using two term perturbation techniques. Numerical values obtained for the problem are expressed in terms of graphs for various flow parameters. Impact of magnetic parameter (M), Casson parameter (β), permeability parameter (K), Grashof number (Gr), modified Grashof number (Gc), Prandtl number (Pr), heat source (Q), radiation parameter (R), chemical reaction (Kr) and Schmidt number (Sc) on the velocity, temperature and concentration profiles are discussed.

Figures 2 and 3 represent the velocity profiles for different values of magnetic parameter (M) and permeability parameter (K) for different values respectively. In Fig. 2 the velocity profile falls with the raising of magnetic parameter values, due to the presence of a magnetic field in an electrically conducting fluid produced Lorentz force that acts against the flow, if the magnetic field applied in the normal direction as within the study. But the reveres trend is observed, the velocity profiles for increasing values of permeability parameter in Fig. 3. It is quite interesting to observe that enhancing values of porosity regime (K), the improved velocity of fluid brought about the boundary layer thickness likewise increment. Velocity distribution for various values of Grashof number (Gr) and modified Grashof number (Gc) are represented in Figs 4-5 respectively as seen in these figures the maximum peak value is obtained in the absence of buoyancy force, this is because of
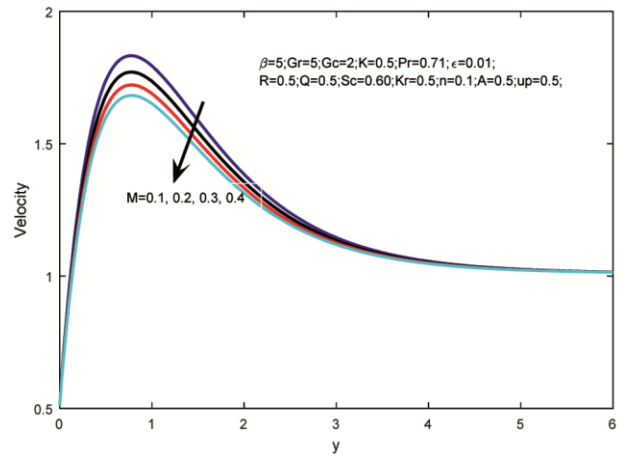

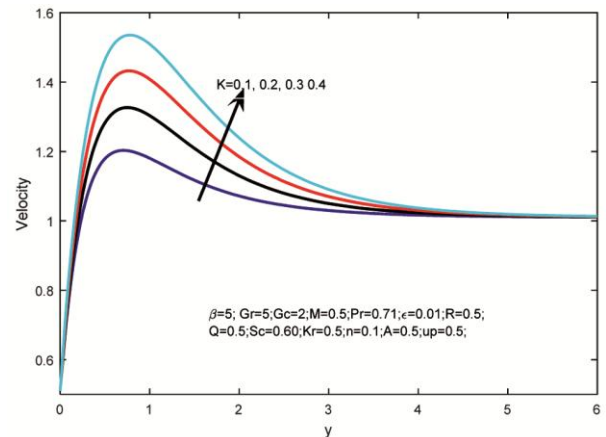Fig.2 — Velocity profiles for different values of magnetic parameter.

Fig. 3 — Velocity profiles for different values of permeability parameter.
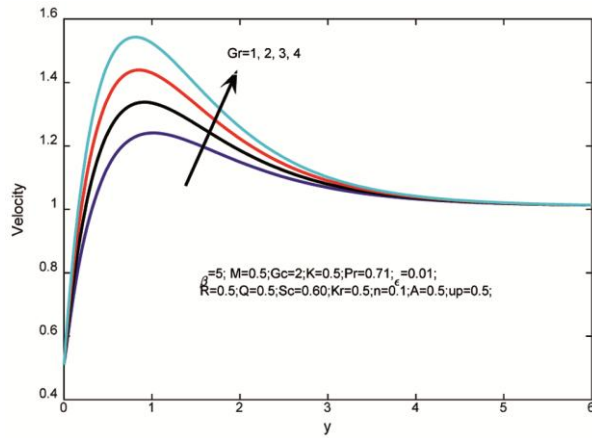
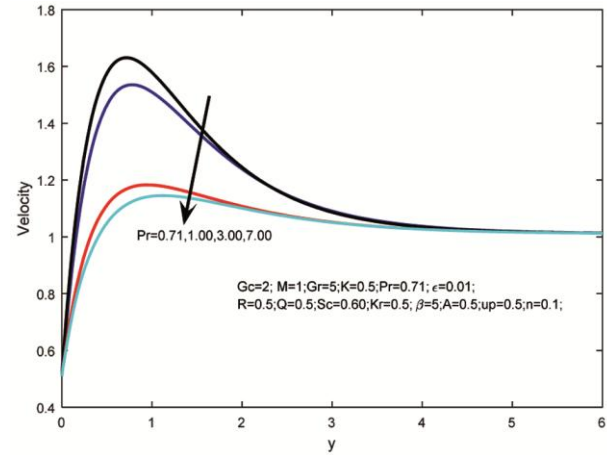Fig. 4 — Velocity profiles for different values of Grashof number.

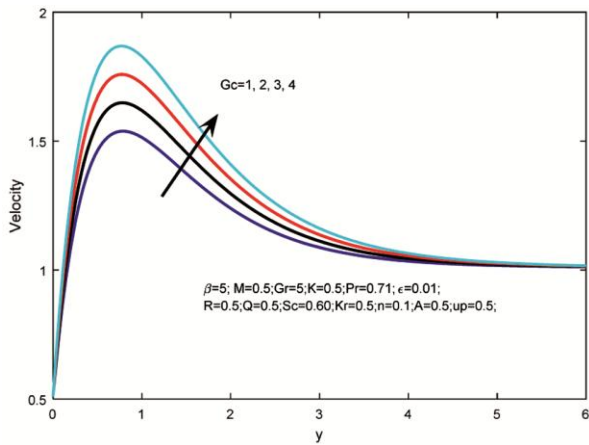Fig. 6 — Velocity profiles for different values of Prandtl number.

Fig. 5 — Velocity profiles for different values of modified Grashof number.
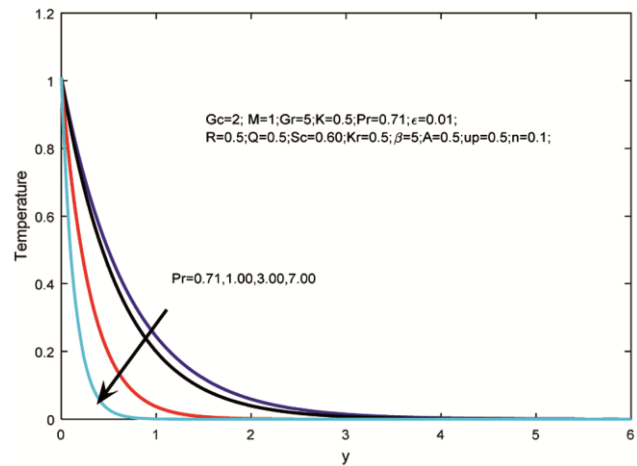

Fig. 7 — Temperature profiles for different values of Prandtl number.

the buoyancy forces improves the boundary layer thickness and the fluid velocity increases in the increasing the values of the Grashof number and modified Grashof number. The impact of Prandtl number (Pr) for the temperature and velocity profiles are as shown in the Figs 6-7 respectively at the temperature and velocity both are decreases for increasing values of Prandtl number, due to smaller values of Prandtl number are similar to raising the thermal conductivities and so heat is ready to decreases far away from the heated surface for greater values of Prandtl number.

The impact of the Casson parameter (β) and the velocity profiles as shown in Fig. 8 it is observed that the velocity profiles increases for increasing values of Casson fluid parameter. due to the effect of cooling of the plate. Figure 9 represent the temperature profiles for various values of heat source/sink parameter (Q), it is noticed that as the value of heat source

parameters increases, the temperature profiles decreases. It is clear that the hydro magnetic boundary layer falls as the heat source/sink effect increase also observed that in the absence of heat absorption the velocity attains maximum peak value. Figure 10 depicts the temperature profiles for dissimilar values of radiation parameter (R), it is observed that for the rising values of radiation parameter, the temperature falls due to the boundary layer wideness. Figures 11 and 12 represent the concentration and velocity profiles for various different values of chemical reaction parameter (Kr). It is noticed that both the concentration and velocity profiles are decreases for increasing value of chemical reaction parameter. For an increase in viscosity of fluid which means velocity boundary layer thickness decreases. Also due to increase in values of Kr , the concentration of fluid particles near the plate drops, which results in decreasing the effect of mass buoyancy forces and
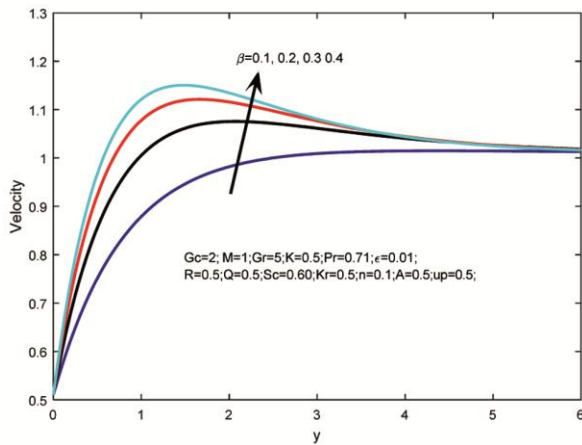
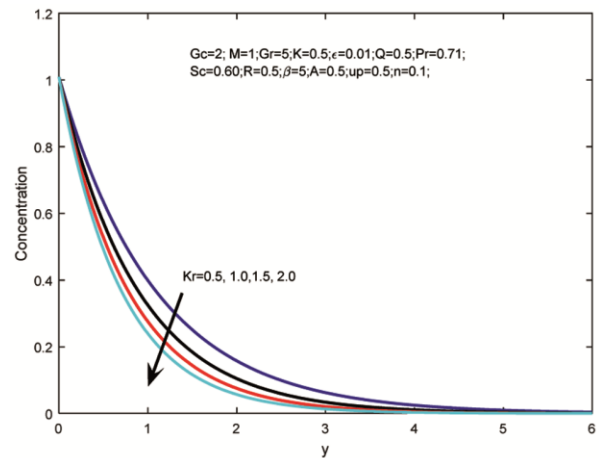Fig. 8 — velocity profiles for different values of Casson parameter.

Fig. 9 — Temperature profiles for different values of heat source parameter.

Fig. 10 — Temperature profiles for different values of radiation parameter.

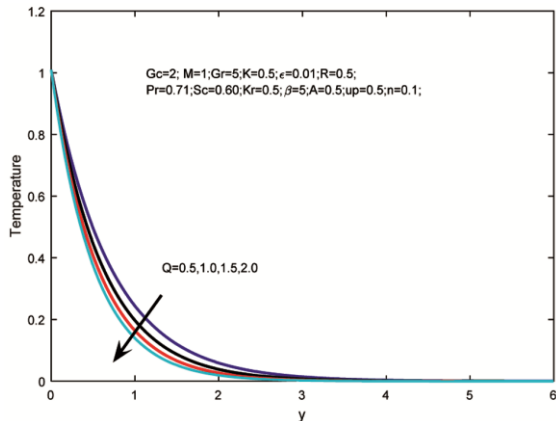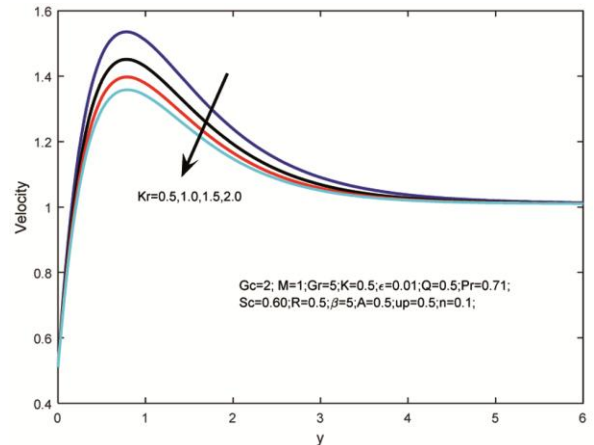Fig.11 — Concentration profiles for different values of Chemical reaction parameter.

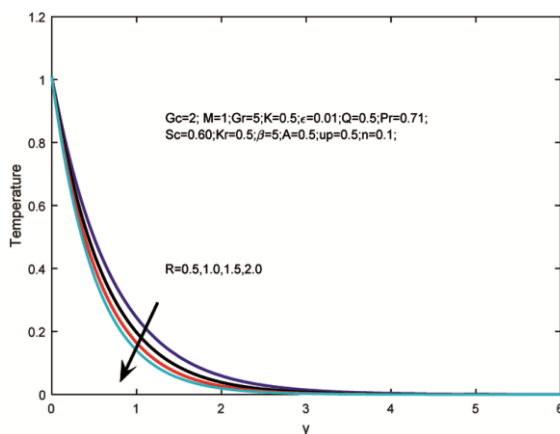Fig. 12 — Velocity profiles for different values of Chemical reaction parameter.

thus decrease the fluid velocity. Due to increase in Kr, the constituents from higher concentration zone moves towards the species in lower concentration zone results of which decreases the concentration boundary layer thickness, thus decreasing the values of concentration. Figures 13 and 14 exhibit the effect of the velocity and concentration profiles for different values of Schmidt number (Sc). It is noticed that both the velocity and concentration profiles are decreases for increasing value of Schmidt number. Because Schmidt number is a dimensionless number defined as the ratio of momentum diffusivity and mass diffusivity, and is used to characterize the fluid flows in which there are simultaneous momentum and mass diffusion convection processes. Figure 15 represents the effect of magnetic parameter (M) on the skin friction profiles. It is noticed that the magnetic parameter increases, decrease the skin-friction. Also it is noticed that from the Figs 16, 17 and 19 that the skin-friction coefficiet increases for the increased values of radiation parameter(R), permeability parameter(K) and chemical reaction parameter(Kr)
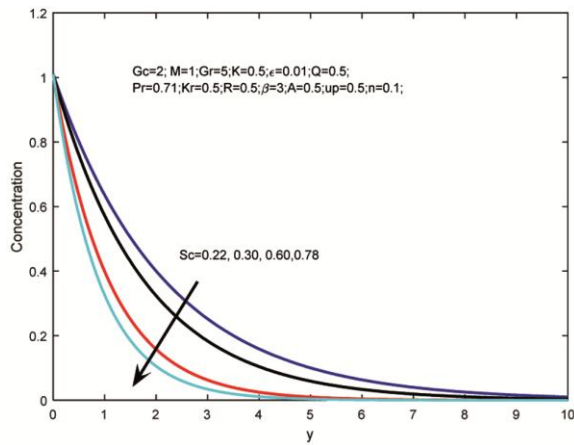
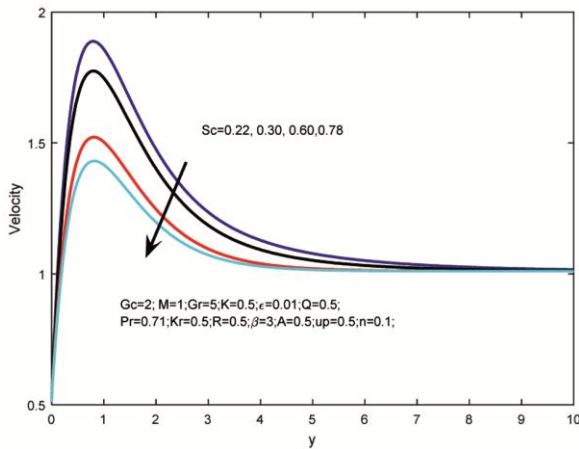Fig. 13 — Concentration profiles for different values of Schmidt number.

Fig. 14 — Velocity profiles for different values of Schmidt number.
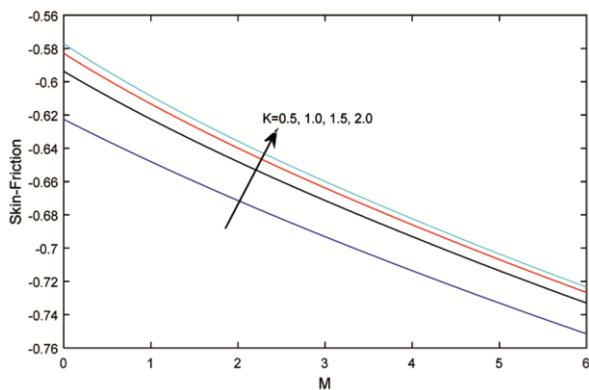

Fig. 15 — Skin friction coefficient for different values of M with K.

Fig. 16 — Skin friction coefficient for different values of K with M.
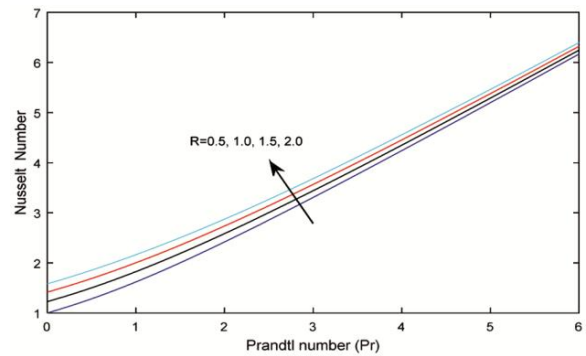
Fig. 17 — Skin friction coefficient for different values of R with Pr.
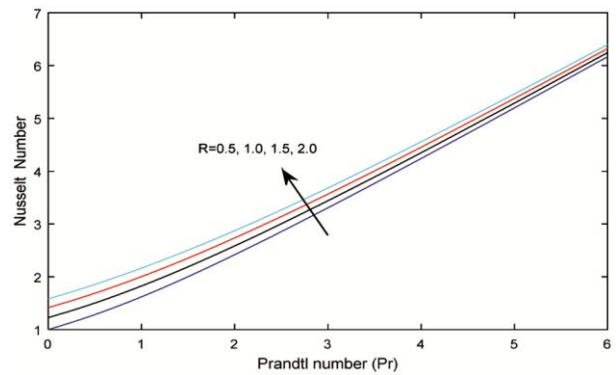
Fig. 18 — Nusselt number for different values of R with Pr.

respectively. Due to the dimensionless shear stress at the surface. Figures 18-20 represent the effect of chemical reaction parameter (Kr) and radiation (R) on the Nusselt number and Sherwood, respectively. It is observed that the Nusselt number and Sherwood number both increases for increasing values radiation and chemical reaction parameter respectively. Because of convection and conduction heat flows are parallel to each other and to the surface normal of the boundary surface, and are all perpendicular to the mean fluid flow and also with the mass transfer option respectively.

The comparison presented in this Table 1 reveal that for the selected values of the parameter (Gc), the values of skin friction determined in this study are in excellent agreement with previously published works.

Fig. 19 — Skin friction coefficient for different values of Kr with Sc.

Fig. 20 — Sherwood number for different values of Kr with Sc.

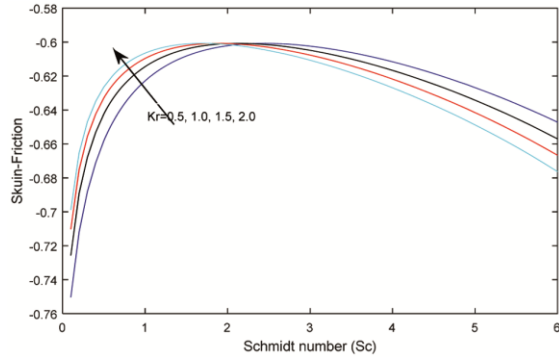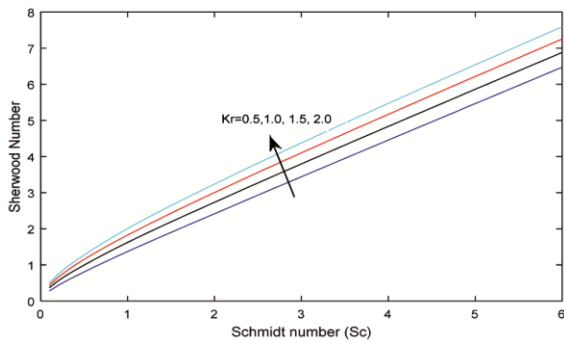Table 1 — Comparison for the numerical values of C_f with previously published data when $Sc = 0.6$, $Pr = 0.71$, $Q = 2$, $\beta = 2$, $Gr = 2$, $K = 0.5$ with $Kr = 0$, $R = 0$.

Gc	Sekhar[4]	Present study
0	2.7200	2..7210
1	3.2772	3.2776
2	3.8343	3.8349
3	4.3915	4.3924
4	4.9487	4.9489

Table 2 report the alterations in skin-friction, Nusselt and Sherwood factors against physical parameters, namely, *M, Kr, Sc, Pr, Q, β , Gr, Gc, K* and *R* respectively. Skin friction falls when raising of the parameters *M, Kr, Sc, Pr, Q, R* but the revers trend is observed in the parameters *β , Gr, Gc, K* Nusselt and Sherwood numbers are decreases with the increase of *Pr, Q, R* and *Kr, Sc* respectively. Nusselt and Sherwood wood numbers being constant when increasing of *M, Kr, Sc, β , Gr, Gc, K* and *M, Pr, Q, β , Gr, Gc, K , R* respectively .

Table 2 — Comparison of C_f Nu & Sh_x for various values of *M, Kr, Sc, Pr, Q, β , Gr, Gc, K, R.*

M	Kr	Sc	Pr	Q	β	Gr	Gc	K	R	C_f	Nu	Sh_x
0.1	0.5	0.6	0.71	0.2	0.5	5	2	0.5	0.5	1.7799	-1.2658	-0.9261
0.5										1.7671	-1.2658	-0.9261
1										1.7573	-1.2658	-0.9261
1	0.5	0.6	0.71	0.2	0.5	5	2	0.5	0.5	1.7573	-1.2658	-0.9261
	1									1.718	-1.2658	-1.1324
	1.5									1.6915	-1.2658	-1.2968
1	0.5	0.22	0.71	0.2	0.5	5	2	0.5	0.5	1.8914	-1.2658	-0.4604
		0.3								1.8531	-1.2658	-0.5664
		0.6								1.7573	-1.2658	-0.9261
1	0.5	0.6	0.71	0.2	0.5	5	2	0.5	0.5	1.7573	-1.2658	-0.9261
			1							1.6859	-1.4769	-0.9261
			3							1.3843	-3.2215	-0.9261
1	0.5	0.6	0.71	0.5	0.5	5	2	0.5	0.5	1.7044	-1.4182	-0.9261
				1						1.6412	-1.6324	-0.9261
				1.5						1.5953	-1.8155	-0.9261
1	0.5	0.6	0.71	0.2	0.1	5	2	0.5	0.5	0.6752	-1.2658	-0.9261
					0.2					1.0478	-1.2658	-0.9261
					0.3					1.3393	-1.2658	-0.9261
1	0.5	0.6	0.71	0.2	0.5	1	2	0.5	0.5	1.1249	-1.2658	-0.9261
						2				1.283	-1.2658	-0.9261
						3				1.4411	-1.2658	-0.9261
1	0.5	0.6	0.71	0.2	0.5	5	1	0.5	0.5	1.569	-1.2658	-0.9261
							2			1.7573	-1.2658	-0.9261
							3			1.9456	-1.2658	-0.9261
1	0.5	0.6	0.71	0.2	0.5	5	2	0.5	0.5	1.7573	-1.2658	-0.9261
								1		1.7839	-1.2658	-0.9261
								1.5		1.8008	-1.2658	-0.9261
1	0.5	0.6	0.71	0.2	0.5	5	2	0.5	0.5	1.7573	-1.2658	-0.9261
									1	1.6763	-1.5087	-0.9261
									1.5	1.6213	-1.7086	-0.9261

8 Conclusions

Numerical results for velocity, temperature and concentration profiles are procured for constant variation of various different ranges and for the different values of the flow significant parameters. The outcomes of the problem are summarized as follows:

(i)   For the increased values of the Permeability parameter (K), Grashof number (Gr), modified Grashof number (Gc) and Casson parameter (β) increase the velocity profiles, but the reverse trend is observed in magnetic parameter(M).

(ii)   The fluid velocity and temperature decreases when Prandtl number (Pr) increases.

(iii)   The Temperature level of the fluid decreases when the Heat source parameter (Q) and Radiation parameter (R) increases.

(iv)   Higher chemical reaction parameter (Kr) and Schmidt number (Sc) causes the numerous reductions in velocity and Concentration profiles.

(v)   With the effect of Permeability parameter, radiation parameter and chemical reaction parameter is to increase the skin-friction coefficient whereas reverse trend is observed with the increase in magnetic parameter and the Nusselt number and Sherwood number increases with the increases of Radiation and Permeability parameter respectively.

References

1   Shehzad S A & Hayat T, *Braz J Chem Eng*, 30 (2013) 187.
2   Vajravelu K & Mukhopadhyay S, *J Hydrodyn,* 25 (2013) 591.
3   Hussanan A & Zuki S M, *PLoS One*, 9 (2014) 10.
4   Sekhar K R & Viswanatha R G, *Chem Process Eng Res*, 39 (2015) 5.
5   Animasaun I L, *J Niger Math Soc*, 34 (2015) 11.
6   Suresh B, Veena P H & Pravin V K, *Int J Eng Sci Res Technol*, 5 (2016), 638.
7   Falodun B O & Fadugba S E, *World Sci News*, 88 (2017) 118.
8   Falodun B O, *Defect Diffusion Forum*, 389 (2018) 18.
9   Hari K Y, Ramana R G V & Makinde O D, *Defect Diffusion Forum*, 389 (2018) 100.
10   Rama K R P & Raju M C, *Int J Pure Appl Math*, 118 (2018) 507.
11   Nagasantoshi P, Ramana R G V, Gnaneswara R M & Padma P, *J Nanofluids*, 7 (2018) 821.
12   Ramana R G V & Hari K Y, *Int J Appl Mech Eng*, 23 (2018) 485.
13   Suneetha K, Ibrahim S M & Ramana R G V, *Multidis Model Mater Struct*, 14 (2018) 1101.
14   Vijaya N, Hari K Y, Kalyani K & Reddy G V R, *Front Heat Mass Transfer*, 11 (2018) 1.
15   Reddy G V R & Hari Krishna Y, *Fluid Dynamics Mater Process*, 14 (2018) 213.